We are IntechOpen, the world's leading publisher of Open Access books Built by scientists, for scientists

4,800
Open access books available

122,000
International authors and editors

135M
Downloads

Our authors are among the

154
Countries delivered to

TOP 1%
most cited scientists

12.2%
Contributors from top 500 universities

CLARIVATE ANALYTICS BOOK CITATION INDEX INDEXED

WEB OF SCIENCE™

Selection of our books indexed in the Book Citation Index in Web of Science™ Core Collection (BKCI)

Interested in publishing with us?
Contact book.department@intechopen.com

Numbers displayed above are based on latest data collected.
For more information visit www.intechopen.com

Chapter 13

Development of a Dimensionless Model for Predicting the Onset of Cavitation in Torque Converters

Darrell Robinette, Carl Anderson and Jason Blough

Additional information is available at the end of the chapter

http://dx.doi.org/10.5772/45793

1. Introduction

The presence of cavitation in any turbomachine can be detrimental to hardware durability, operating performance or noise and vibration characteristics. In an automatic transmission, the torque converter has the potential to cavitate under specific operating conditions resulting in a degradation in torque transfer, irregular engine speed regulation, blade damage or noise complaints depending on the degree of cavitation. Recent trends in planetary automatic transmissions are towards an increased number of fixed gear states and an expanding area of torque converter lockup clutch operation to reduce fuel consumption. The result is a reduction in the packaging volume available for the torque converter torus as indicated in Fig. 1 and the requirement to accommodate the increasing specific torque output of down sized, boosted engines. This combination of torus design and engine matching increases the opportunity for cavitation with higher toroidal flow velocities, higher pressure differentials across blade surfaces and greater power input to the fluid during normally inefficient operating points.

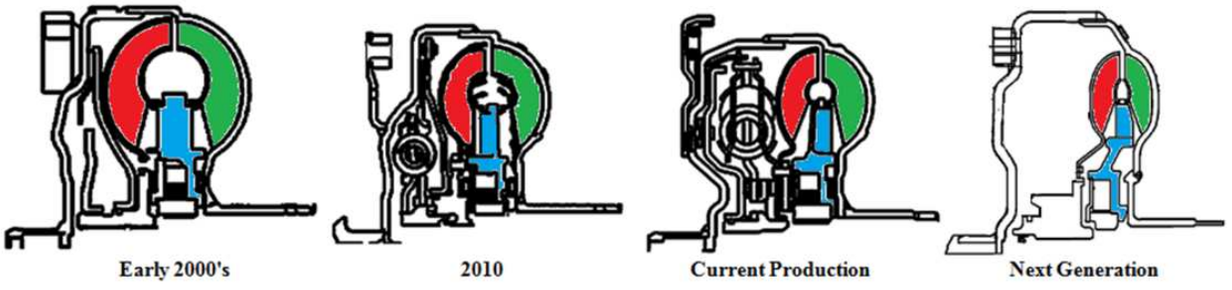

Figure 1. Recent design trend in automotive torque converter torus dimensions; pump (green), turbine (red) and stator (blue)

The onset of cavitation can be readily identified by a distinct change in radiated sound from the torque converter during particular driving maneuvers. Advanced stages of cavitation are distinguished by a loss of torque transfer through the torque converter and unexpected engine speed regulation due to the presence of large scale multi-phase flow structures. The focus of this chapter will be on incipient cavitation and detecting the onset of cavitation rather than on advanced stages of cavitation. The chapter will detail an experimental technique for acoustically detecting onset of cavitation in torque converters of varying designs and performance characteristics over a range of operating points. The effects of torque converter design parameters and operating conditions on cavitation are quantified through dimensional analysis of the test results. The objective is to develop a tool for designing converters with minimal cavitation by fitting power product and response surface models to the dimensionless data. Initially, torque converter designs following exact geometric similitude are analyzed. The constraint of similitude are relaxed in subsequent model iterations to allow application of the dimensional analysis and model fitting process to a broader range of converter designs. Empirical power product and response surface models were produced capable of predicting the onset of cavitation with less than 10% and 7% error, repectively, for a large population of torque converters.

2. The torque converter and cavitation

2.1. Torque converter design and performance

The torque converter is a particular class of turbomachine that utilizes a pressurized fluid circulating through multiple bladed elements that add or extract energy from the fluid. The torque converter is the powertrain component that couples the engine crankshaft to the gear system of the automatic transmission, allowing the transfer of power. It serves a number of other purposes, including decoupling the engine and transmission, allowing engine idle without the aid of a clutch, multiplying torque at low engine speeds to overcome poor self-starting capability of the internal combustion engine and regulation of engine speed during vehicle acceleration.

The torque converter pump, connected to the engine crankshaft, rotates at engine speed and torque, increases the angular momentum of the toriodal fluid as it flows from inner to outer torus radius. The toroidal fluid then flows into the turbine where its angular momentum is decreased and torque is transferred to the automatic transmission via the turbine shaft. The toriodal fluid exits the turbine and enters the stator which redirects the fluid at a favorable angle back into the pump. The redirection of the fluid increases the angular momentum of the fluid reducing the amount of increase required by the pump, thereby multiplying torque.

Dimensionless parameters are frequently used in the turbomachinery field to relate fundamental design characteristics to performance such as speed, torque, flow or head. The torque converter is no exception and uses a semi-dimensionless parameter known as K-factor,

$$K = \frac{N_p}{\sqrt{T_p}} \tag{1}$$

where N_p and T_p represent pump speed and pump torque, respectively, to characterize a specific design of the torus and bladed elements. A dimensionless form of K-factor can be formulated by including fluid density and torus diamter to form unit input speed,

$$U = K\sqrt{\rho D^5} \ . \tag{2}$$

Unit input speed is the inverse square of the torque coefficienct, which is more commonly found in turbomachinery. The value of K-factor or unit input speed are single value functions of the ratio of turbine (output) speed to pump (input) speed, referred to as speed ratio,

$$SR = \frac{N_t}{N_p} \ . \tag{3}$$

Torque ratio, the ratio of turbine to pump torque (see Eq. 4), quantifies torque multiplication of a design and is a single value of function of speed ratio.

$$TR = \frac{T_t}{T_p} \tag{4}$$

Efficiency of the torque converter is also used to quantify performance and is the product of speed ratio and torque ratio. Figure 2 summarizes the typical hydrodynamic performance attribtues of K-factor, TR and efficiency as a function of SR. At zero turbine speed (SR=0), referred to as stall, K-factor and TR are constant regardless of pump speed. As SR increases TR decreases monotonically until the coupling point is reached and is unity thereafter. K-factor in general will remain approximately constant until a threshold SR where it begins to increase gradually up to coupling and then asymptotically approaches infinite capacity as SR nears unity.

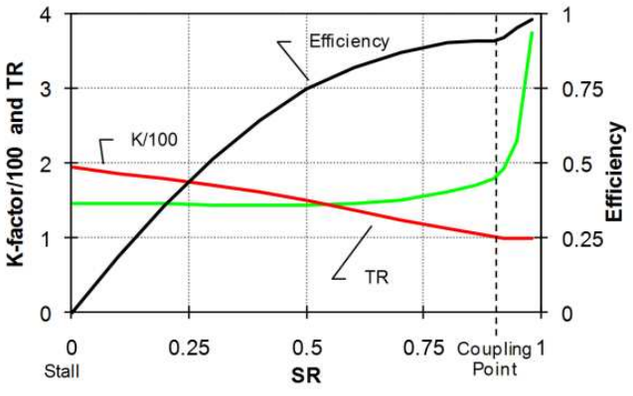

Figure 2. Typical dimensionless and semi-dimensionless performance characteristics of a hydrodynamic torque converter

2.2. Cavitation in torque converters

The change in angular momentum across the pump, turbine or stator produces a torque acting on individual blades that is equal to the product of the local static pressure and radius from converter centerline integrated over the entire surface area of the blade. A pressure differential exists between low and high pressure surfaces of a blade and in order for an increase in torque transfer to occur, the pressure differential across the blade surface in each element must increase. At a critical torque level, the localized pressure on the low pressure side of a blade will drop below the vapor pressure of the toroidal fluid, causing the nucleation of cavitation bubbles. Stall, SR=0, is most susceptible to the occurrence of cavitation due to the combination of high toroidal flow velocities, high incidence angle at element inlets and the thermal loading of the fluid. Cavitation may also occur while climbing a steep grade, repeated high throttle launches or during initial vehicle launch towing a heavy load. The discussion in this chapter will be focued on cavitation while operating at the stalled condition.

Incipient cavitation produces a negligible effect on overall torque converter performance due to a small volume of two phase flow in a localized region of the toroidal flow circuit. Continued operation at moderate to heavy cavitation will begin to cause a departure from the idealized K-factor relationship as an increased volume of toroidal flow is displaced by vapor. Previous testing by [1] found that heavy and sustained cavitation will cause an approximate 3% decrease in pump torque at stall. The onset of cavitation could more precisely be detected by a noted increase in the fluctuating component of pressure using in-situ pressure taps and a microwave telemetry technique, see [1]. The testing conducted at stall showed that a sudden increase in the ensemble averaged fluctuating pressure measurements signified the onset of cavitation for a particular charging pressure. Pressure measurements at the leading edge of the stator blade by [8] showed the fluctuating component of pressure to damp out as cavitation occurred as the cavitation structure formed at the leading edge of the stator blade. These results were confirmed by CFD work performed through [3], showing that the leading edge of the stator is indeed the initial nucleation site for cavitation at stall. As pump speed increased further, the size of the cavitation region grew at the leading edge of the stator blade.

The collapse of cavitation bubbles produces a broadband noise and may become objectionable to vehicle occupants. The radiated noise can also be used to identify the onset of cavitation as found by [4]. Using an acoustically treated test fixture, the onset of cavitation was readily found by an abrupt increase in filtered sound pressure level (SPL) above a critical pump speed. Utilizing a non-contact measurement technique facilitates testing of multiple torque converter designs, however, the size of the test fixture limited the testing to a single diameter torus and element designs spanning a narrow 23 K-factor point range. A dimensionless model for predicting pump speed at onset of cavitation was developed by [5] for this data, however, was not practical to predict cavitation for a diverse torque converter design population. The goal of this investigation was to utilize a similar nearfield acoustical measurement technique and test a general design population of torque converters at stall to determine the operating threshold

at incipient cavitation. Through dimensional analysis, this data would be used to develop a comprehensive design tool capable of predicting the onset of cavitation with reasonable accuracy.

3. Experimental setup

3.1. Dynamometer test cell

A torque converter dynamometer test cell was constructed with an acoustically treated test fixture to acquire nearfield acoustical measurements to identify the onset of cavitation. The dynamometer setup consisted of four major subsystems as shown in Fig. 3; a hydraulic supply system, drive dynamometer, acoustical test fixture, and an absorbing dynamometer with an optional stall plate to prevent rotation. The hydraulic system has setpoint control of the charge pressure and back pressure imposed upon the torque converter as well as regulation of the temperature of the automatic transmission fluid at the inlet to the test fixture. A 215 kW direct current drive dynamometer was used to simulate typical engine speeds and torques. The 225 kW absorbing dynamometer was connected to the stall plate to prevent rotation and induce the stall operating condition. The acoustical test fixture was sized to accommodate at least 150 mm of acoustical foam to improve measurement coherence and allow torque converter designs of widely varying torus dimensions. Two data acquisition systems (not shown) were used to acquire data. One for operating data (speed, torque, pressure, temperature, flow, etc.) at a 1 kHz sample rate and one for nearfield microphone and pump speed data at a sample rate of 51.2 kHz.

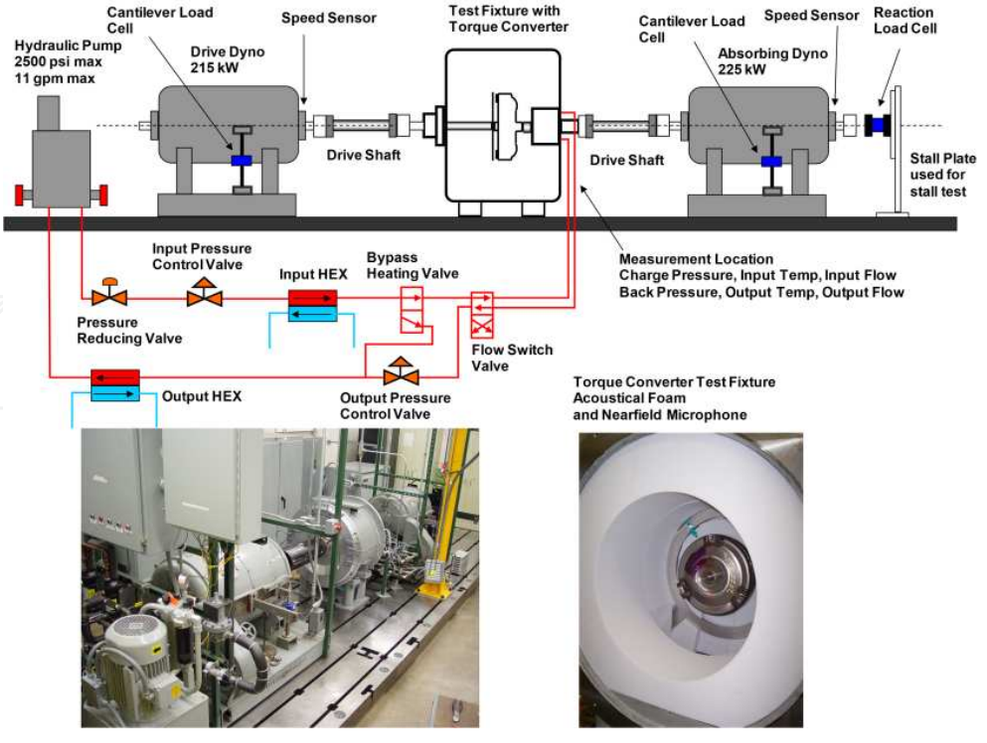

Figure 3. Torque converter dynamometer test cell and acoustically treated test fixture with nearfield microphone measurement

3.2. Stall cavitation test

A standardized test procedure for the stall operating condition was developed to transition each torque converter tested from a noncavitating to cavitating condition. Starting at 500 rpm, pump speed was sweep at 40 rpm/s until a speed sufficiently higher than onset of cavitation (~ 1200 to 2300 rpm). Fourteen stall speed sweep tests at various combinations of charge pressures ranging from 483 to 896 kPa, delta pressures between 69 to 345 kPa and input temperatures of 60, 70 and 80 ˚C were completed for each torque converter tested. The range of operating points tested is contained in Table 1.

	Low	High
Charge Pressure	483 kPa	896 kPa
Back Pressure	69 kPa	345 kPa
Input Temperature	60 ˚C	80 ˚C

Table 1. Range of operating point pressures and temperatures tested

3.3. Acoustical detection of incipient of cavitation

A sample nearfield acoustical measurement during a stall speed sweep test is shown in Fig. 4, in both the time domain (a) and frequency domain (b). The subtle change in SPL near 1400 rpm and frequency characteristic above 6 kHz correlates to the collapse of incipient cavitation bubbles. All torque converters tested exhibited similar behaviour when onset of cavitation occurs. Similar findings have been reported by [2] and [7] for incipient cavitation and acoustical detection techniques in rotating machinery.

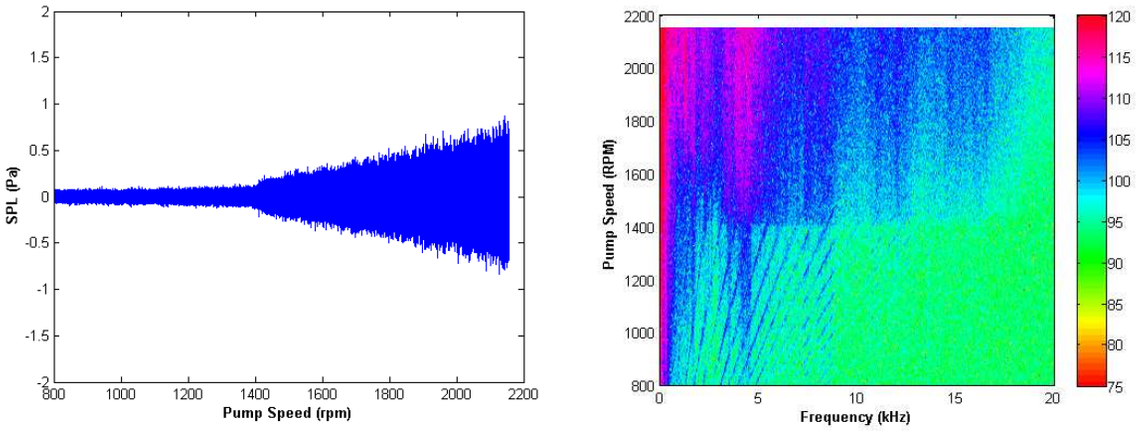

a) Time domain b) Frequency domain

Figure 4. Time (a) and frequency (b) domain nearfield acoustical measurement for standardized stall speed sweep cavitation test

To eliminate subjectivity in identifying the exact pump speed at onset of cavitation, a standardized signal processing technique was developed to reduce the nearfield acoustical measurements shown in Fig. 4 into a signal that more readily indicates the onset of cavitation. A 6 kHz Kaiser window high pass filter was first applied to the nearfield microphone data to remove noise unrelated to cavitation. The filtered SPL was then time averaged at 40 equally spaced points throughout the stall speed sweep test, resulting in Fig. 5a. Post processing the data in this manner showed an abrupt increase in filtered SPL to occur at a particular pump speed that is taken as the onset of cavitation for this investigation. A metric referred to as slope^2, see Fig. 5b, was computed and used in an automated algorithm to identify the exact pump speed at which cavitation occurred using a threshold criteria of a 12.5% increase. This value was found to give an accuracy of +/- 40 rpm with 95% confidence across the broad range of converter designs and operating points tested. The details regarding the experimental setup, post processing and identifying the exact pump speed at onset of cavitation can be found in [10].

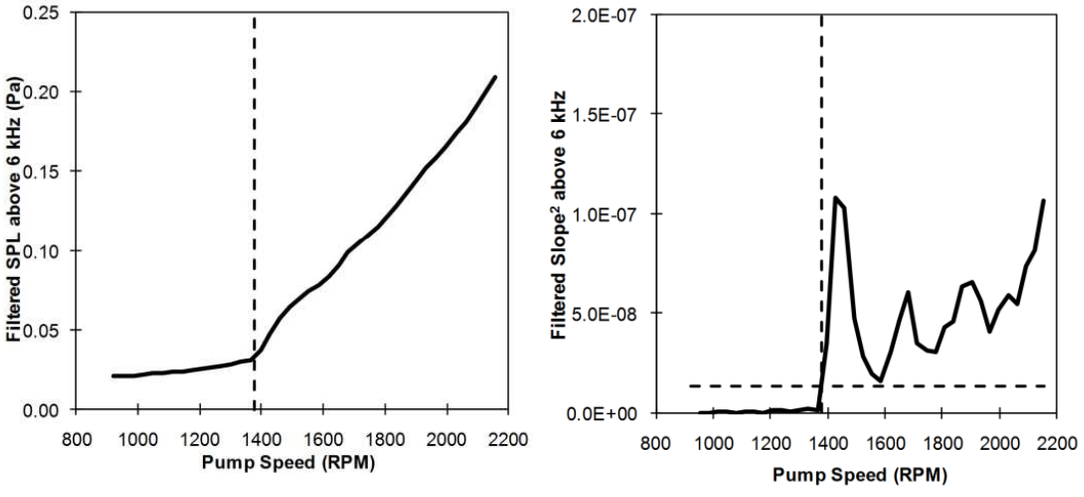

a) Filtered SPL

b) Filtered slope^2

Figure 5. Filtered SPL (a) and slope^2 (b) post processed from nearfield acoustical measurements to identify pump speed at onset of cavitation

3.4. Experimental torque converters

Fifty one torque converters were tested for this investigation of varying design characteristics that would satisfy the performance requirements of a wide range of powertrain applications. Although each torque converter differed geometrically in some respect, each design followed a common philosophy of torus and bladed element design to achieve certain performance attributes. The torque converter designs were arranged into four major populations, from exact geometric similitude to a general design population including all 51 torque converters with no similitude. Six diameters were tested in this investigation and will be denoted D_1 through D_6. D_1 corresponds to the smallest diameter at slightly smaller than 240 mm and D_6 the largest diameter at slightly larger than 300 mm. The

details of the torque converters within each design population will be discussed later in the chapter as dimensionless quantities when the empirical models for predicting the onset of cavitation are presented. The exact designs characteristics will be omitted or presented as dimensionless quantities for proprietary reasons.

4. Dimensional analysis

4.1. Non-dimensionalizing onset of cavitation

Analysis of geometrically similar torque converter designs was performed to determine if the onset of cavitation could be non-dimensionalized using diameter and other relevant parameters. Such a dimensionless quantity would allow experimentally determined incipient cavitation thresholds for a given diameter, element design and operating point to be scaled to multiple diameters when exact dimensional scaling and operating point are preserved. The two torque converters considered are of exact geometric scaling with diameters D_2 and D_6, with the same stall unit input speed of 140 and stall torque ratio of 2.0. The designs only differ in pump blade count, which was necessary to maintain identical unit input speed.

Due to the relationship between speed and torque, either quantity could be used to describe the critical operating threshold at the onset of cavitation. Torque, however, is a more relevant quantity than speed as torque capacity is a more useful quantity when performing torque converter and powertrain matching and is fundamentally related to the pressure drop across the blades of the pump, turbine and stator. Stator torque at the onset of cavitation, $T_{s,i}$ was selected over pump or turbine torque for comparing critical cavitation stall operating thresholds as previous research by [3] and [8] showed cavitation to originate at the leading edge of the stator blade. Stator torque can generically be written as,

$$T_s \propto n_{sb}\left(A_{blade}\Delta p\right)r \tag{5}$$

where n_{sb} is the number of stator blades, A_{blade}, the surface area of an individual blade, Δp, the pressure differential between high and low pressure sides and r, the radius from centreline. In general, smaller diameter torque converters will begin cavitating at higher pump speeds, but lower elements torques relative to a larger geometrically scaled torque converter design. This can readily be seen in the plots of filtered SPL versus pump speed (a) and stator torque (b) in Fig. 6.

The critical stator torque at incipient cavitation will primarily depend on design parameters and fluid properties, most notably a characteristic size dimension and the fluid pressure imposed upon the toroidal flow. Figure 7 is a plot of $T_{s,i}$ versus the average of the controlled charge and back pressures for all fourteen operating conditions. It is clear from Fig.7 that diameter and average pressure significantly influence the onset of cavitation. The stator torque threshold at cavitation was found to be 95 to 118 Nm greater than the smaller diameter with 95% confidence, as reported by [10].

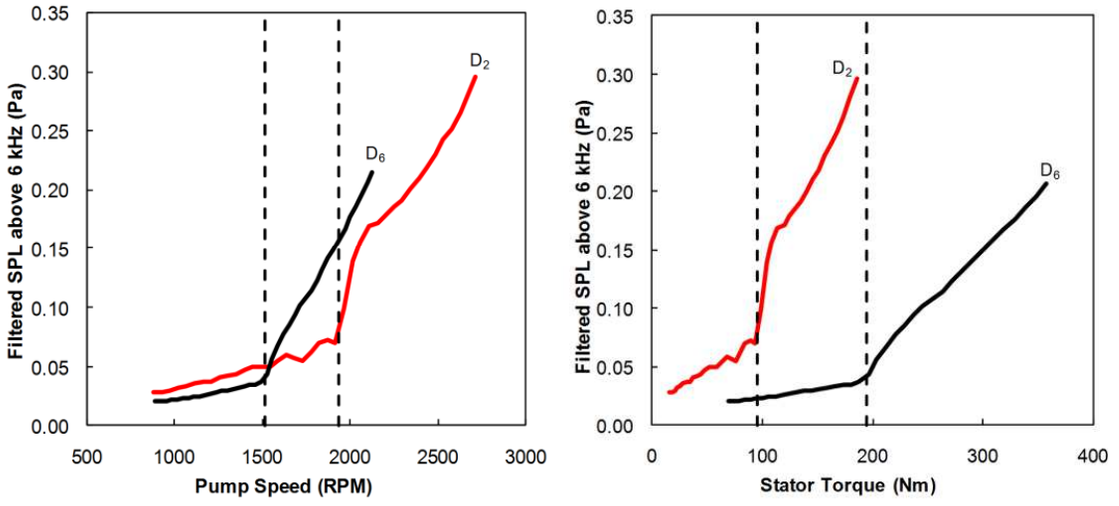

a) Pump speed b) Stator torque

Figure 6. Filtered SPL versus pump speed (a) and stator torque (b) at the onset of cavitation

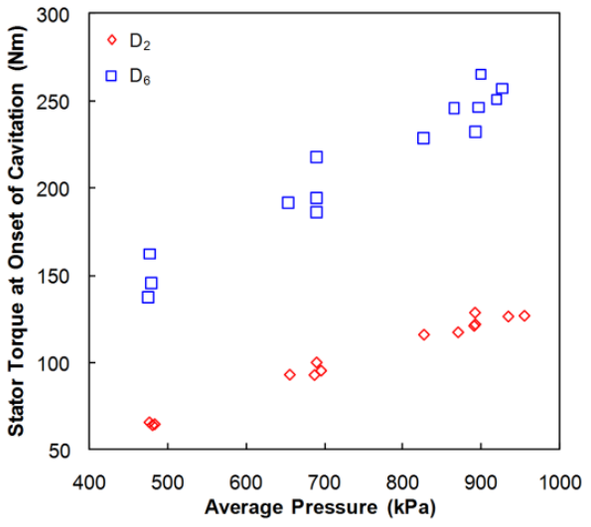

Figure 7. Stator torque at onset of cavitation versus average absolute pressure imposed upon the toroidal flow for geometrically scaled torque converters

These observations lead to the development of a dimensionless quantity by [11] incorporating stator torque at the onset of cavitation, $T_{s,i}$, diameter, D and average pressure, p_{ave} as given by Eq. 6.

$$\frac{T_{s,i}}{D^3 p_{ave}} \tag{6}$$

This quantity will be referred to as dimensionless stator torque and represents a similarity condition when geometric similitude is observed. Thus, stator torque cavitation threshold can be scaled to another diameter when the same stall operating point is maintained. The similarity condition for dimensionless stator torque is expressed by,

$$\left(\frac{T_s}{D^3 p_{ave}}\right)_1 = \left(\frac{T_s}{D^3 p_{ave}}\right)_2 \tag{7}$$

where the subscript 1 represents the known cavitation threshold and diameter and subscript 2 represents the cavitation threshold and diameter that are to be scaled. For Eq. 7 to hold true the average pressure, the combination of charge and back pressures, must be equivalent to properly scale the stator torque threshold. When the ratio of average pressures becomes unity it can subsequenctly be dropped from Eq. 7. The similarity condition for dimensionless stator torque is illustrated clearly in Fig. 8 when filtered SPL is plotted versus dimensionless stator torque. For the geometrically scaled designs at the the same operating point, onset of cavitation reduces to approximately the same value of dimensionless stator torque, as indicated by the vertical dashed lines. A difference of 1.7% between dimensionless stator torque values at incipient cavitation was found.

Alternatively pump speed could be used to formulate a similarity condition using dimensionless pump at onset of cavitation, Eq. 8, as proposed by [1]. This dimensionless quantity incorporates the critical pump speed threshold at cavitation, $\omega_{p,i}$, with diameter, D, the charging pressure imposed upon on the toroidal flow, p_c, and automatic transmission fluid density, ρ. The onset of cavitation occurs at nearly the same value of dimensionless pump speed as seen in Fig. 9.

$$\Omega_{i,p} = \frac{\omega_{p,i} D}{\sqrt{p_c/\rho}} \tag{8}$$

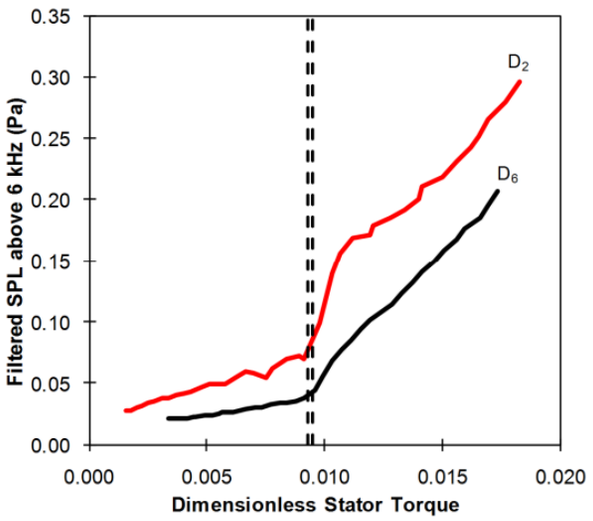

Figure 8. Filtered SPL versus dimensionless stator torque for geometrically scaled torque converters, dashed lines indicate onset of cavitation

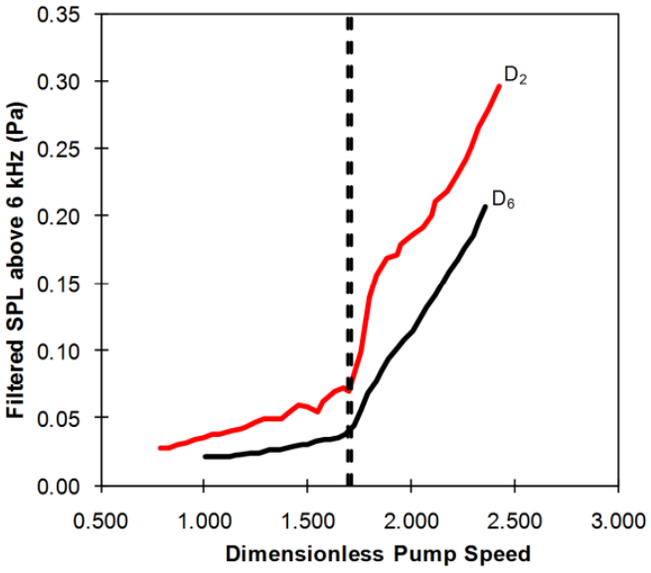

Figure 9. Filtered SPL versus dimensionless pump speed for geometrically scaled torque converters, dashed lines indicate onset of cavitation

4.2. Pi group formulation

The dimensional analysis and formation of pi groups for onset of cavitation in torque converters is initiated by formulating a list of regressor variables that will be fit to the response variable in developing empirical models. The response variable, stator torque at the onset of cavitation, can be described by the regressor variables that determine the boundary value problem of the toroidal flow for incipient cavitation at stall. The list of variables will include those that describe the torque converter design and those related to the operating conditions of the fluid. The design variables that principally determine the stator torque cavitation threshold at stall include the diameter, D, axial length, L_t, and element blade designs comprising the pump, turbine and stator. Element blade design manifests itself as the integrated quantities of K-factor and TR. Both of these quantities correlate to cavitation behaviour at stall, see [10], and their simplicity is favored over a lengthy list of individual blade design parameters. The number of stator blades as well as their shape can strongly influence performance and therefore the onset of cavitation. The airfoil shape of the stator blade is described by the ratio of blade maximum thickness, t_{max}, and chord length, l_c, and has been shown to have a statistically significant effect on the stator torque cavitation threshold, see [10]. The pressures imposed upon the torque converter are included in the list of variables for the dimensional analysis. As

found by [10], increasing charging pressure can alter the stator torque cavitation threshold at stall by as much as 150 Nm for a particular design. Secondary variables that affect the cavitation threshold are those describing the thermal conditions of the toroidal flow, namely cooling flow rate, Q, and the automatic transmission fluid properties of density, ρ, viscosity, μ, specific heat, C_p, and thermal conductivity, k. Rather than using charge and back pressures, average pressure, p_{ave}, and pressure drop, Δp, will be used as they implicitly comprehend the cooling flow rate through the toroidal flow. Equation 9 gives the list of primary and secondary varies that determine $T_{s,i}$ in a torque converter,

$$T_{s,i} = f\left(D, L_t, K, TR, n_{sb}, t_{\max}, l_c, p_{ave}, \Delta p, \rho, \mu, C_p, k\right). \tag{9}$$

The dimensionless form of Eq. 9 was resolved into dimensionless stator torque as a function of dimensionless design parameters and dimensionless operating point parameters using the PI Theroem with repeating variables of D, p_{ave}, ρ and C_p. The exponents for the repeating variables contained in each pi group are found using,

$$\Psi = -\mathbf{Q}\mathbf{P}^{-1} \tag{10}$$

where $\mathbf{\Psi}$, $\mathbf{Q}$ and $\mathbf{P}$ are 10x4, 10x4 and 4x4 matrices. The rows of $\mathbf{P}$ are the repeating variables D, p_{ave}, ρ and C_p, while the rows of $\mathbf{Q}$ are the remaining variables, $T_{s,i}$, L_t, K, TR, n_{sb}, t_{max}, l_c, Δp, μ, and k from Eq. 9. The columns of both $\mathbf{P}$ and $\mathbf{Q}$ represent the dimensions of M, L, t and θ. A $\mathbf{\Pi}$ group matrix, Eq. 11, is formed by combining the $\mathbf{\Psi}$ matrix and a 10x10 identity matrix, $\mathbf{I}$, in which the diagonal represents the remaining variables, $T_{s,i}$, Lt, K, TR, n_{sb}, t_{max}, l_c, Δp, μ, and k raised to the power of 1. Each row of Eq. 11 represents a Π group, while the columns are the variables from Eq. 9 in the following order, D, p_{ave}, ρ, C_p, $T_{s,i}$, L_t, K, TR, n_{sb}, t_{max}, l_c, Δp, μ, and k. The cells of the matrix in Eq. 11 are the exponents assigned to each variable. Equation 12 lists the Π groups found using this method.

$$\mathbf{\Pi} = [\,\mathbf{\Psi}, \mathbf{I}\,] = \begin{array}{c} \\ \Pi_1 \\ \Pi_2 \\ \Pi_3 \\ \Pi_4 \\ \Pi_5 \\ \Pi_6 \\ \Pi_7 \\ \Pi_8 \\ \Pi_9 \\ \Pi_{10} \end{array} \left[\begin{array}{cccc:cccccccccc} D & p_{ave} & \rho & C_p & T_{s,i} & L_t & K & TR & n_{sb} & t_{max} & l_c & \Delta p & \mu & k \\ \hline -3 & -1 & 0 & 0 & 1 & 0 & 0 & 0 & 0 & 0 & 0 & 0 & 0 & 0 \\ -1 & 0 & 0 & 0 & 0 & 1 & 0 & 0 & 0 & 0 & 0 & 0 & 0 & 0 \\ 2.5 & 0 & 0.5 & 0 & 0 & 0 & 1 & 0 & 0 & 0 & 0 & 0 & 0 & 0 \\ 0 & 0 & 0 & 0 & 0 & 0 & 0 & 1 & 0 & 0 & 0 & 0 & 0 & 0 \\ 0 & 0 & 0 & 0 & 0 & 0 & 0 & 0 & 1 & 0 & 0 & 0 & 0 & 0 \\ -1 & 0 & 0 & 0 & 0 & 0 & 0 & 0 & 0 & 1 & 0 & 0 & 0 & 0 \\ -1 & 0 & 0 & 0 & 0 & 0 & 0 & 0 & 0 & 0 & 1 & 0 & 0 & 0 \\ 0 & -1 & 0 & 0 & 0 & 0 & 0 & 0 & 0 & 0 & 0 & 1 & 0 & 0 \\ -1 & -0.5 & -0.5 & 0 & 0 & 0 & 0 & 0 & 0 & 0 & 0 & 0 & 1 & 0 \\ -1 & -0.5 & -0.5 & -1 & 0 & 0 & 0 & 0 & 0 & 0 & 0 & 0 & 0 & 1 \end{array}\right]. \tag{11}$$

$$\begin{aligned}
\Pi_1 &= \frac{T_{s,i}}{D^3 p_{ave}} \\
\Pi_2 &= \frac{L_t}{D} \\
\Pi_3 &= K\sqrt{\rho D^5} \\
\Pi_4 &= TR \\
\Pi_5 &= \frac{t_{\max}}{D} \\
\Pi_6 &= \frac{l_c}{D} \\
\Pi_7 &= n_{sb} \\
\Pi_8 &= \frac{\Delta p}{p_{ave}} \\
\Pi_9 &= \frac{\mu}{D\sqrt{\rho p_{ave}}} \\
\Pi_{10} &= \frac{k}{D\sqrt{\rho p_{ave}} C_p}
\end{aligned} \tag{12}$$

A new dimensionless quantity, stator blade thickness ratio, is formed by combining Π_5 and Π_6. The Prandlt number is formed with the combination of Π_9 and Π_{10} to quantify thermal effects. The list of variables that effect stator torque at the onset of cavitation found in Eq. 9 are now made dimensionless as summarized in Eq. 13 as a function of dimensionless stator torque,

$$\frac{T_{s,i}}{D^3 p_{ave}} = f\left(\frac{L_t}{D}, U, TR, n_{sb}, \frac{t_{\max}}{l_c}, \frac{\Delta p}{p_{ave}}, \Pr\right) \tag{13}$$

where the five dimensionless design parameters are torus aspect ratio, L_t/D, unit input speed, U, stall torque ratio, TR, number of stator blades, n_{sb}, and stator blade thickness ratio, t_{max}/l_c. The two dimensionless operating point parameters are dimensionless operating pressure, $p_{ave}/\Delta p$, and the Prandlt number. These seven dimensionless parameters will be used to form empirical models on dimensionless stator torque.

Not all the dimensionless design parameters of Eq. 13 are necessary when considering the various populations of the torque converter designs considered in this investigation. When exact geometric similitude is observed, all five dimensionless design parameters are constant and only the dimensionless operating point parameters are used to fit a model. Those dimensionless design parameters that remain constant are removed from Eq. 13 before a model is fit to the data. As the constraint of geomertric similitude is relaxed, dimensionless design parameters are added back into Eq. 13 before proceeding fit a model to the data.

5. Dimensionless models

5.1. Model functions

The power product method (PPM) and response surface methodology (RSM) were used to develop relationships between dimensionless stator torque and the dimensionless design and operating point parameters of Eq. 13. The power product method has been traditionally used as the standard model function for most dimensionless prediction models found in fluid mechanics and heat transfer. The response surface method, however, is a statistical approach to developing a linear regression. An empirical power product and response surface model will be developed for each of the four torque converter populations of varying geometric similitude.

The power product model function is given by Eq. 14, with $\hat{y}$ equal to predicted dimensionless stator torque and Π representing the dimensionless parameters on the right hand side of Eq. 13. The model error, ε, is the difference between measured and predicted dimensionless stator torque. The exponents, b_i, and coefficient, b_0, were found using a Gaussian-Newton numerical search technique based upon minimizing ε; see [11] for more details.

$$\hat{y} = b_0\left(\prod_{i=1}^{k} x_i^{b_i}\right) + \varepsilon \tag{14}$$

A second order function was assumed for the RSM used in this investigation, which contains linear, quadratic and two factor interactions as used by [12]:

$$\hat{y} = b_0 + \sum_{i=1}^{k} b_i \Pi_i + \sum_{i=1}^{k} b_{ii} \Pi_i^2 + \sum_{i=1}^{k-1} \sum_{j=i+1}^{k} b_{ij} \Pi_i \Pi_j + \varepsilon \,. \tag{15}$$

The response parameter, as with the PPM, is dimensionless stator torque and the regressors, Π, are the dimensionless design and operating point parameters of Eq. 13. The coefficients for the RSM were found using least squares method by minimizing the error between experimentally measured, y, and predicted, $\hat{y}$,dimensionless stator torque. Equation 15 can be written in matrix form as

$$\hat{\mathbf{Y}} = \mathbf{X}\mathbf{b} + \boldsymbol{\varepsilon} \tag{16}$$

where $\hat{\mathbf{Y}}$ is a vector of predicted dimensionless stator torque, $\mathbf{X}$ is a matrices of the dimensionless regressors, $\mathbf{b}$ is a matric of the regression coefficients and $\boldsymbol{\varepsilon}$ is a vector of error. The regression coefficents are found using Eq. 17, where $\mathbf{Y}$ replaces $\hat{\mathbf{Y}}$ and $\boldsymbol{\varepsilon}$ is omitted.

$$\mathbf{b} = \left(\mathbf{X}^T\mathbf{X}\right)^{-1}\mathbf{X}^T\mathbf{Y} \tag{17}$$

A stepwise regression technique was used to produce a response surface model with the minimum number of dimensionless regressors that were statisically significant as

determined by a 95% joint Bonferroni confidence interval and *t*-test. The initial model only included the b_0 coefficient. During the stepwise regression, regressors were added or removed from the model dictated by the statistical criterion described. The reduction in model error realized by the addition of any one regressor was dependent upon the regressors already included in the model. Use of the stepwise regression procedure can greatly reduce the number of regressors, thereby complexity of the model while increasing the amount of variation in the response explained. It should be noted that the dimensionless parameters of *U* and Pr were divided by 1000 for the RSM so that the estimated regression coefficients were of roughly the same magnitude. For a more detailed description of the linear and stepwise regression techniques utilized, the reader is referred to [6] and [9].

The accuarcy and goodness of fit for both the PPM and RSM models were determined by computing the root mean square error (RMSE) and the linear association between the dimensionless response and regressors. RMSE is an estimator of a models standard deviation and for this investigation was computed as a percentage, denoted as %RMSE. Equation 18 defines %RMSE, where *n* is the number of data points and *p*, the number of regressors in the model. A value of %RMSE of 10% or less can generally be regarded as providing an empirical dimensionless model with acceptable accuracy.

$$\%RMSE = \sqrt{\frac{\sum_{i=1}^{n}\left(\frac{y_i - \hat{y}_i}{y_i} * 100\right)^2}{n-p}} \tag{18}$$

A measure of the proportionate amount of variation in the response explained by a particular set of regressors in the model is the adjusted coefficient of multiple determination, R^2_a:

$$R_a^2 = 1 - \frac{\sum_{i=1}^{n}\left(y_i - \hat{y}_i\right)^2 \Big/ \left(n-p\right)}{\sum_{i=1}^{n}\left(y_i - \bar{y}\right)^2 \Big/ \left(n-1\right)}. \tag{19}$$

This metric will calculate to a value between 0 and 1, with values of 0.85 or higher signifying a model that accurately represents the data. R^2_a is generally preferred over R^2, the coefficient of multiple determination, as it is a better evaluator of model variation and the number of regressors present. Whereas R^2 will always increase in value when additional regressors are added to a model, R^2_a may increase or decrease depending on whether or not the additional regressors actually reduce the variation in the response.

5.2. Exact geometric similitude

Two torque converters of exact geometric scaling with diameters D_2 and D_6 were considered for developing a dimensionless prediction model for onset of cavitation at stall. The

functional form of Eq. 13 contains only the dimensionless operating point parameters since the dimensionless design parameters are equivalent for both diameters. Equations 20 and 21 are the PPM and RSM models for torque converters with exact similitude and are graphically represented in Fig. 10a and 10b, respectively. The values of the dimensionless design parameters for the two torque converters considered for exact geometric similitude are provided in Fig 10.

$$\frac{T_{s,i}}{D^3 p_{ave}} = b_0 \left[\left(\frac{\Delta p}{p_{ave}} \right)^{b_1} (\mathrm{Pr})^{b_2} \right] \tag{20}$$

$$\frac{T_{s,i}}{D^3 p_{ave}} = b_0 + b_1 \left(\frac{\Delta p}{p_{ave}} \right)^2 + b_2 (\mathrm{Pr})^2 \tag{21}$$

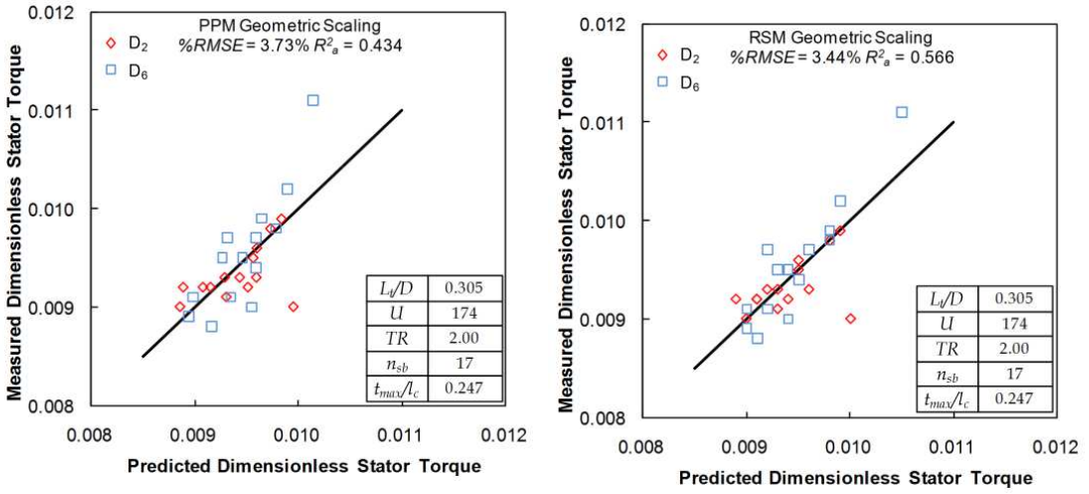

a) PPM b) RSM

Figure 10. Dimensionless stator torque PPM (a) and RSM (b) for exact geometric scaling of a torque converter design for a range of operating points

The model diagonistics provided at the top of each model plot shows %RMSE below 4% and R^2_a above 0.43. The RSM model performance is slightly better than that of the PPM with a 9% decrease in %RMSE and a 23% increase in R^2_a. Although both the PPM and RSM models have an %RMSE below 4%, R^2_a does not meet the 0.85 criteria for a good model fit with sufficient explanation of response variation for the regressors in the model. Use of dimensionless stator torque results in a constant value when geometric similitude is observed and an identical operating point is considered. For the range of dimensionless operating points tested, see Table 2, a small variation in dimensionless stator torque resulted which does not particularly lend itself to empirical modeling, requiring a greater variation in the dimensionless quantities to adequately define a curve. However, even with relatively low values of R^2_a, the prediction accuracy for scaling stator torque cavitation thresholds for a given torus and set of element designs is high.

	Low	High
Average Pressure	481 kPa	963 kPa
Pressure Drop	69 kPa	345 kPa
Prandlt Number	116	300

Table 2. Range of dimensionless operating point parameters tested

5.3. Torus scaling

For the torus scaling population, three torque converters with varying L_t/D ratios were used to investigate the ability to apply dimensional analysis and develop a predictive model with reasonable accuracy when geometric similitude is not observed. The element designs of the three converters were maintained, with the exception of stator blade count for the D_5 converter, such that unit input speeds remained constant. The PPM and RSM models are given by Eq. 22 and 23 and include the dimensionless design parameters of torus aspect ratio and number of stator blades to account for the design variations:

$$\frac{T_{s,i}}{D^3 p_{ave}} = b_0 \left[\left(\frac{L_t}{D} \right)^{b_1} \left(n_{sb} \right)^{b_2} \left(\frac{\Delta p}{p_{ave}} \right)^{b_3} \left(\mathrm{Pr} \right)^{b_4} \right] \tag{22}$$

$$\frac{T_{s,i}}{D^3 p_{ave}} = b_0 + b_1 \left(\frac{\Delta p}{p_{ave}} \right) + b_2 \left(\frac{L_t}{D} \right)^2 + b_3 \left(\frac{L_t}{D} \right) \left(\frac{\Delta p}{p_{ave}} \right) + b_4 \left(\frac{L_t}{D} \right) \left(\mathrm{Pr} \right) + b_5 \left(n_{sb} \right) \left(\frac{\Delta p}{p_{ave}} \right). \tag{23}$$

Figure 11a and 11b contain the PPM and RSM models, respectively, for the torus scaling popualtion and include the model performance metrics and dimensionless design parameters. An increase in the range of dimensionless stator torque can be noted over the exact geometric similitude population shown in Figure 10a and 10b. The PPM model experienced a negligible increase in %RMSE and a doubling of R^2_a when compared with the exact geometric scaling PPM model. A decrease in %RSME from 3.44% to 2.87% and an increase in R^2_a from 0.566 to 0.926 was realized compared to the geometric scaling RSM model. Both model functions increase the amount of variation in dimensionless stator torque accounted for by the regressors in the model. The RSM model has a slight advantage over the PPM model due to the statistical nature of determining which dimensionless parameters to include. This can be seen grpahically in Fig. 11 in that the data fits the RSM model closer for all three diameters versus the PPM model. The utility of these particular models for predicting $T_{s,i}$ are limited to the element blade design (fixed U and TR) tested in Fig. 11, but can be sacled to other diameters as long as the L_t/D ratio remains between 0.29 and 0.317.

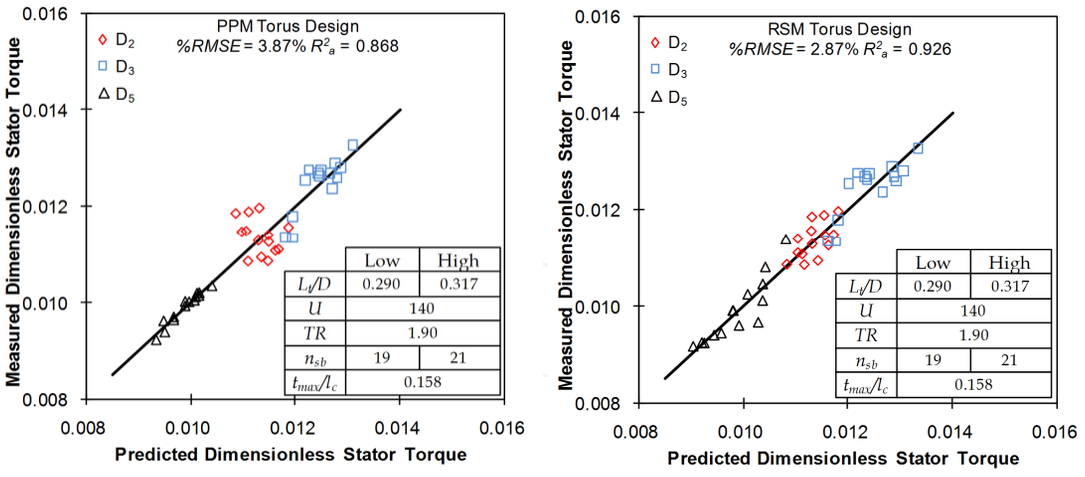

a) PPM b) RSM

Figure 11. Dimensionless stator torque PPM (a) and RSM (b) for torus geometry scaling of a torque converter design for a range of operating points

5.4. Pump and stator

The dimensionless PPM and RSM models for a population in which pump and stator designs varied for a fixed L_t/D are given by:

$$\frac{T_{s,i}}{D^3 p_{ave}} = b_0 \left[(U)^{b_1} (TR)^{b_2} (n_{sb})^{b_3} \left(\frac{t_{\max}}{l_c} \right)^{b_4} \left(\frac{\Delta p}{p_{ave}} \right)^{b_5} (\mathrm{Pr})^{b_6} \right] \tag{24}$$

and

$$\frac{T_{s,i}}{D^3 p_{ave}} = b_0 + b_1 \left(\frac{t_{\max}}{l_c} \right) + b_2 (U)^2 + b_3 (TR)^2 + b_4 (n_{sb})^2 + b_5 \left(\frac{\Delta p}{p_{ave}} \right)^2 + b_6 (\mathrm{Pr})^2 + b_7 (U)(TR) + \ldots$$
$$\ldots + b_8 (U) \left(\frac{t_{\max}}{l_c} \right) + b_9 (n_{sb}) \left(\frac{t_{\max}}{l_c} \right). \tag{25}$$

Sixteen torque converter designs with an L_t/D of 0.3 were formed from various combinations of 5 pump and 11 stator designs. The dimensionless design parameters of U, TR, n_{sb} and t_{max}/l_c are required to characterize the effect pump and stator design have on toriodal flow and incipient cavitation, while L_t/D was eliminated as it remained fixed. The %RMSE for both the PPM and RSM models increased approximately 2.25% over the torus scaling population models. This is to be expected as more data points are included, departing further from geometric similitude. Although the torque converter designs are more varied, R^2_a increased for both model functions indicating that the additional dimensionless design parameters helped to explain the variation in dimensionless stator torque. With %RMSE's of roughly 6% and 5% and R^2_a greater than 0.92, both models are

accurate for design purposes. Predicted dimensionless stator torque from either model can be scaled to another diameter if the L_t/D ratio of 0.3 is maintained and the elements design falls within the scope of the dimensionless design parameters used to develop the model.

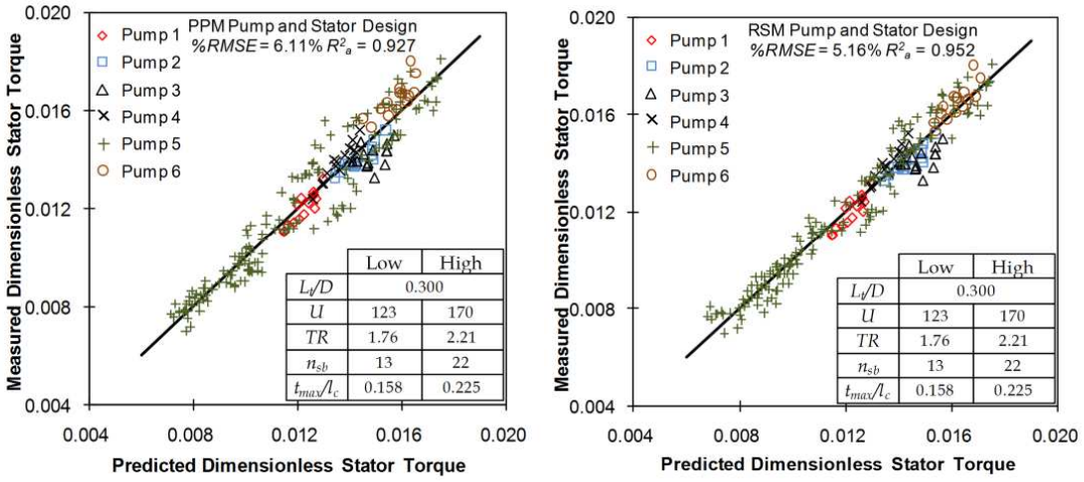

a) PPM b) RSM

Figure 12. Dimensionless stator torque PPM (a) and RSM (b) for various pump and stator geometry for a given torque converter torus design for a range of operating points

5.5. General design

For the general design population of torque converters, variations in torus and element blade geometries were considered to develop a PPM and RSM model for predicting $T_{s,i}$ at stall. All of the dimensionless design parameters in Eq. 13 were required to develop the PPM and RSM models, as all varied for the matrix of designs tested. The PPM model, Eq. 26, contains 7 dimensionless parameters and 8 regression coefficients, while the RSM model, Eq. 27, contains 18 dimensionless parameters as determined by the stepwise regression procedure and 19 regression coefficients.

$$\frac{T_{s,i}}{D^3 p_{ave}} = b_0 \left[\left(\frac{L_t}{D} \right)^{b_1} (U)^{b_2} (TR)^{b_3} (n_{sb})^{b_4} \left(\frac{t_{\max}}{l_c} \right)^{b_5} \left(\frac{\Delta p}{p_{ave}} \right)^{b_6} (\mathrm{Pr})^{b_7} \right] \tag{26}$$

$$\frac{T_{s,i}}{D^3 p_{ave}} = b_0 + b_1 \left(\frac{L_t}{D} \right) + b_2 (U) + b_3 (TR) + b_4 (n_{sb}) + b_5 \left(\frac{t_{\max}}{l_c} \right) + b_6 \left(\frac{L_t}{D} \right)^2 + b_7 (n_{sb})^2 + \ldots$$

$$\ldots + b_8 \left(\frac{t_{\max}}{l_c} \right)^2 + b_9 \left(\frac{\Delta p}{p_{ave}} \right)^2 + b_{10} (\mathrm{Pr})^2 + b_{11} \left(\frac{L_t}{D} \right) (n_{sb}) + b_{12} \left(\frac{L_t}{D} \right) \left(\frac{t_{\max}}{l_c} \right) + b_{13} (U)(TR) + \ldots . \tag{27}$$

$$\ldots + b_{14} (U)(n_{sb}) + b_{15} (U) \left(\frac{t_{\max}}{l_c} \right) + b_{16} (TR)(n_{sb}) + b_{17} (TR) \left(\frac{t_{\max}}{l_c} \right) + b_{18} (n_{sb}) \left(\frac{t_{\max}}{l_c} \right)$$

Figure 13a and 13b are the PPM and RSM models for a general population of torque converter desgins plotted as measured versus prediceted dimensionless stator torque. The model diagonistics of %RMSE and R^2_a are included in Fig 13 along with the range of dimensionless design parameters of the converter designs. The range of the dimensionless operating parameters remained the same as those reported in Table 2.

Either form of the general design population empirical model, PPM or RSM, demonstrates the capability to be used in the design process to predict onset of cavitation for a torque converter at stall. %RMSE is below and R^2_a is above the threshold criteria of what was deemed acceptable for an accurate and useable model. The RSM model, with it's statistically determined functional form and increased number of dimensionless regressors, resulted in a closer curve fit model than the PPM as seen in Fig. 13, particularly at the extreme values of dimensionless stator torque. The RSM model's %RMSE of 6.52% and R^2_a of 0.936 demonstrates that an accurate model for predicting a complex flow phenomenon such as onset of cavitation in a turbomachine when geometric similitude is greatly relaxed can be developed. The scope of the empirical PPM or RSM models are limited to the range of dimensionless design parameters reported in Fig. 13 to achieve prediction $T_{s,i}$ values within the %RMSE's noted.

Figure 14 is a histogram of the residual errors, ε, for the general torque converter design PPM and RSM models. For both empirical models the errors do not significantly deviate from normalcy and follows that of a normal distribution. Although both models have error well distributed around zero, the RSM shows a narrower and taller distribution, indicating that the RSM model prediction capability exceeds that of the PPM model. This is reinforced by the %RMSE and R^2_a model diagnostics.

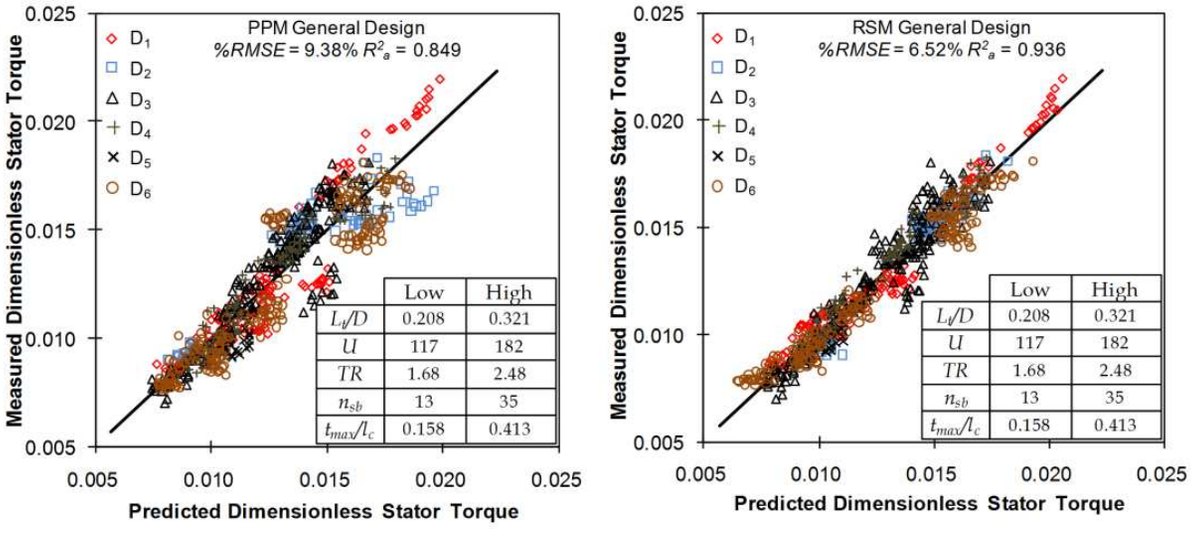

a) PPM b) RSM

Figure 13. Dimensionless stator torque PPM (a) and RSM (b) for a general design population of torque converters for a range of operating points

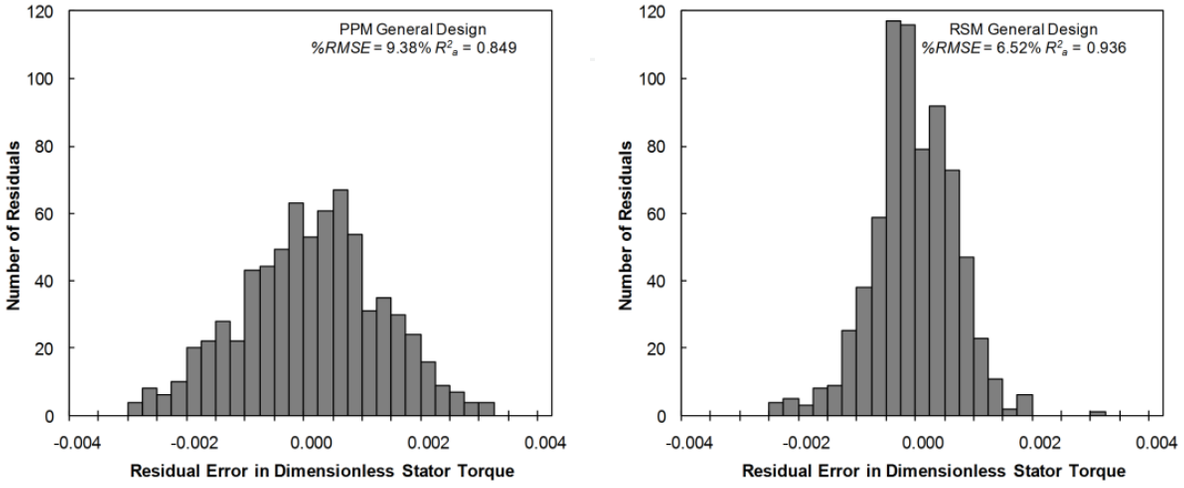

a) PPM

b) RSM

Figure 14. Histogram for general design PPM (a) and RSM (b) model residual error

The span of the experimental data for the 6 diameters, encompassing 51 torque converter designs are presented in Fig. 15 as pump power at the onset of cavitation. As Fig. 15 shows, the onset of cavitation occurs within a consistent range of pump power, between 10 and 65 kW, across the range of diameters tested. In general, a torque converter design with a low K-factor and high TR operating at a high average pressure will transition to cavitation at a higher value of pump power. It is worth noting that incipient cavitation does not occur at moderate or heavy pump power, but rather at moderate to low power levels. This indicates that any given torque converter design has a high potential to cavitate lightly or moderately during typical driving conditions at or near stall. As discussed previously, incipient or light cavitation does not hinder performance or component durability. The objective then of the torque converter engineer is to design the torque converter to operate in a wider speed-torque range cavitation free to prevent conditions of heavy and sustained cavitation during atypical driving conditions.

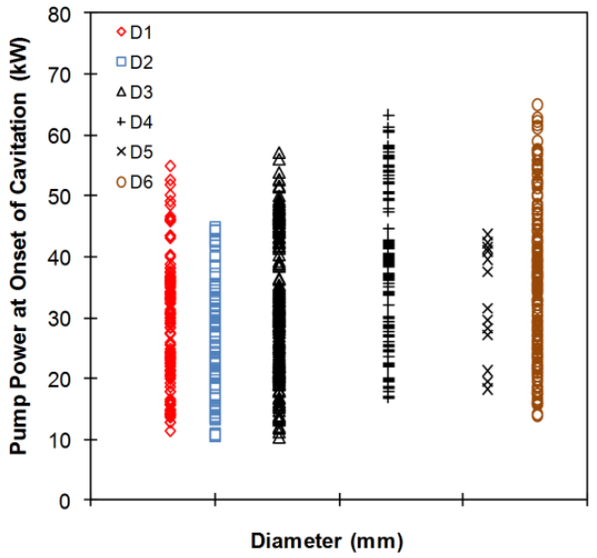

Figure 15. Power at onset of cavitation for general design population of torque converters

Pump torque is the principal parameter used when performing torque converter and engine matching as it is directly equivalent to engine torque. During the design phase of a torque converter and subsequent engine matching, Eq. 28 would be used to take the predicted value of stator torque at the onset of cavitation from Eq. 26 or 27 to calculate pump torque at onset of cavitation. This enables the torque converter engineer to better formulate a design that balances performance requirements and minimize cavitation potential when matching to the torque characteristics of a specific engine.

$$T_{p,i} = \frac{T_{s,i}}{TR-1} \tag{28}$$

5.6. Model summary

Table 3 compares each PPM and RSM model developed for the four torque converter design populations. As geometric similitude decreases the number of dimensionless regressors required to realize a highly accurate model increases for either the PPM or RSM model. This is an expected trend as the numerous interactions between design parameters become increasingly important in determining stator torque at the onset of cavitation while stalled. The increase in R^2_a confirms this conclusion as the variation in the data is nearly completly explained by the addition of the dimensionless design parameters. The gradual increase in %RMSE from exact geometric similitude to a general design population is not substantial enough to qualify either the PPM or RSM models to be in accurate or deficient for design purposes. The regression coefficients for all of the PPM or RSM models have been purposefully omitted from this chapter as they were derived from proprietary torque converter designs whose performance attributes could otherwise be extracted.

			RSM			PPM		
Population	Similitude	Data Points	Regressors	RMSE (%)	R^2_a	Regressors	RMSE (%)	R^2_a
Exact Similitude	Exact	28	3	3.34	0.566	3	3.73	0.434
Torus Scaling	Elements	42	6	2.87	0.926	5	3.87	0.868
Pump and Stator Design	Torus	224	10	5.16	0.953	7	6.037	0.929
General Design	None	714	19	6.52	0.936	8	9.38	0.849

Table 3. Summary of PPM and RSM models predictive capability by torque converter design population

6. Conclusions

The chapter presents experimentally obtained values for stator torque at the onset of cavitation for torque converters of greatly varying geometric similitude nondimensionalized and used as dimensionless reponse and regressors for developing empirical models. Power product method (PPM) and response surface method (RSM) models were curve fit using regression techniques to dimensionless stator torque as a function of dimensionless design and operating point parameters. PPM and RSM models created from data sets of decreasing geometric similitude showed that R^2_a values above 0.85 are achieved even with greatly relaxed geometric similitude. The %RMSE values resulting for each PPM or RSM model of decreasing geometric similitude were not substantial enough to indicate inadequacies in the dimensional analysis or data modeling methodology. A RSM model was presented which is capable of predicting $T_{s,i}$ for general torque converter design with a %RMSE of 6.52%. This error is deemed sufficiently low and its scope of prediction large enough to rate the RSM model a valuable tool for optimizing torus and element geometries with respect to the onset of cavitation at stall in three element torque converters. The next phase of this research will be to expand testing to include non stall conditions to determine the desinent (disappearance) point of cavitation and non-dimensionalize the test data into an equivalent design tool.

Appendix

Nomenclature

C_p	Specific heat (kJ/kg·K)
D	Diameter (m)
K	K-factor (rpm/Nm$^{0.5}$)
L_t	Axial length (m)
N_p	Pump speed
Pr	Prandlt number
Q	Volumetric flow rate (m^3/s)
R^2_a	Adjusted coefficient of multiple determination
$T_{p,i}$	Pump torque at onset of cavitation (Nm)
$T_{s,i}$	Stator torque at onset of cavitation (Nm)
SR	Speed ratio
TR	Torque ratio
U	Unit input speed
%RMSE	Percent root mean square error
b	Regression coefficient
k	Thermal conductivity (W/m·K)
l_c	Chord length (m)
n_{sb}	Number of stator blades
p_{ave}	Average pressure (kPa)
p_b	Back pressure (kPa)
p_c	Charge pressure (kPa)
Δp	Delta pressure (kPa)
t_{max}	Maximum blade thickness (m)
$\hat{y}$	Predicted dimensionless response
y	Measured dimensionless response
ε	Model residual error
ρ	Density (kg/m^3)
μ	Viscosity (N·s/m^2)
$\omega_{p,i}$	Pump speed at onset of cavitation (rad/s)
θ	Temperature (°C)

Author details

Darrell Robinette
General Motors LLC, USA

Carl Anderson and Jason Blough
Michigan Technological University,
Department of Mechanical Engineering – Engineering Mechanics, USA

7. References

[1] Anderson, C., Zeng, L., Sweger, P. O., Narain A., & Blough, J., "Experimental Investigation of Cavitation Signatures in an Automotive Torque Converter Using a Microwave Telemetry Technique," in Proceedings of the 9th International Symposium on Transport Phenomena and Dynamics of Rotating Machinery (ISROMAC '02), Honolulu, Hawaii, USA, February 2002

[2] Courbiere, P., "An Acoustical Method for Characterizing the Onset of Cavitation in Nozzles and Pumps," *in Proceedings of the 2nd International Symposium on Cavitation Inception*, New Orleans, La, USA, December 1984

[3] Dong, Y., Korivi, V., Attibele, P. & Yuan, Y., "Torque Converter CFD Engineering Part II: Performance Improvement Through Core Leakage Flow and Cavitation Control," *in Proceedings of the SAE World Congress and Exhibition*, Detroit, Mich, USA, March 2002, 2002-01-0884

[4] Kowalski, D., Anderson, C. & Blough, J., "Cavitation Detection in Automotive Torque Converters Using Nearfield Acoustical Measurements," *in Proceedings of the SAE International Noise and Vibration Conference and Exhibition (SAE '05)*, Grand Traverse, Mich, USA, May 2005, 2005-01-2516

[5] Kowalski, D., Anderson, C. & Blough, J., "Cavitation Prediction in Automotive Torque Converters," *in Proceedings of the SAE International Noise and Vibration Conference and Exhibition (SAE '05)*, Grand Traverse, Mich, USA, May 2005, 2005-01-2557

[6] Kutner, M. H., Nachtsheim, C. J. & Neter, J., *Applied Linear Regression Models*, McGraw-Hill, New York, NY, USA, 4th edition, 2004

[7] McNulty, P. J. & Pearsall, I., "Cavitation inception in pumps," *Journal of Fluids Engineering*, vol. 104, no. 1, pp. 99–104, 1982

[8] Mekkes, J., Anderson, C. & Narain, A., "Static Pressure Measurements on the Nose of a Torque Converter Stator during Cavitation," *in Proceedings of the 10th International Symposium on Transport Phenomena and Dynamics of Rotating Machinery (ISROMAC '04)*, Honolulu, Hawaii, USA, February 2004

[9] Montgomery, D. G., *Design and Analysis of Experiments*, 6th Edition, John Wiley and Sons Inc., 2005

[10] Robinette, D., Anderson, C., Blough, J., and Johnson, M., Schweitzer, J. & Maddock D., "Characterizing the Effect of Automotive Torque Converter Design Parameters on the Onset of Cavitation at Stall," *in Proceedings of the SAE International Noise and Vibration Conference and Exhibition (SAE '07)*, St. Charles, Ill, USA, May 2007, 2007-01-2231

[11] Robinette, D., Schweitzer, J., Maddock D., Anderson, C., Blough, J., & Johnson, M., "Predicting the Onset of Cavitation in Automotive Torque Converters Part I: Designs with Geometric Similitude," *International Journal of Rotating Machinery*, Vol. 2008

[12] Robinette, D., Schweitzer, J., Maddock D., Anderson, C., Blough, J., & Johnson, M., "Predicting the Onset of Cavitation in Automotive Torque Converters Part II: A Generalized Model", *International Journal of Rotating Machinery*, Vol. 2008